Project 2 – Modeling of a Three-Phase Induction Machine

Saumil Pradhan
International Center for Automotive Research (CU-ICAR)
Clemson University
Clemson, SC, USA
saumilv@clemson.edu

Pranav Ghate
Holcombe Department of Electrical Engineering
Clemson University
Clemson, SC, USA
pghate@clemson.edu

Leticia Breton
Electrical Engineering Exchange Student
Clemson University
Clemson, SC, USA
leticib@clemson.edu

Sahand Liasi
Holcombe Department of Electrical Engineering
Clemson University
Charleston, SC, USA
liasi@clemson.edu

Shubham Gupta
International Center for Automotive Research (CU-ICAR)
Clemson University
Clemson, SC, USA
gupta9@clemson.edu

***Abstract*—Induction machines are popular for various applications. Their simplicity has earned them a place among several applications. Hence this project is an effort to formulate the mathematical model of an induction machine through its characteristic equations. The implementation is carried out in MATLAB(R2021b)/Simulink environment. The induction machine is simulated under free acceleration, which denotes a no-load condition or zero load torque on the machine's shaft. The mathematical model uses the ABC frame and follows the principles of Faraday's laws of electromagnetism and Newton's law. To demonstrate the dynamic response of the induction machine to the changes in excitation, the simulation results, including the current, rotor speed, and electromagnetic torque, are presented and discussed. Further analysis includes the review of peak values of some critical machine variables, power consumption, and the losses involved in the conversion. This analysis goes a long way in explaining the ramifications of machine behavior on some remaining components of the drive system.**

***Index Terms*—Induction machine, modeling, power analysis**

I. Nomenclature

This table contains the exhaustive list of notations used throughout this paper.

TABLE I
LIST OF NOTATIONS

Quantity	Description	Units
v	Voltage	V
i	Current	A
r	Resistance	Ohms (Ω)
L	Winding inductance	H
X	Winding reactance	Ohms (Ω)
ω_E	Excitation frequency	rad/s
f	Excitation frequency in Hz	Hz
λ	Flux linkage	Wb.t
p	Heaviside notation	-
N	Number of turns of winding	-
N_s	Synchronous speed	rev/min
Φ	Angular position of stator or rotor	rad
θ_r	Angular displacement of rotor	rad
ω_r	Angular speed of rotor	rad/s
ω_B	Base speed of the machine	rad/s
J	Rotor inertia	kg.m^2
T_e	Electromagnetic torque	Nm
T_L	Load torque	Nm
B	Shaft damping coefficient	Nms/rad
P	Number of stator poles	-

II. Introduction

Induction motors are standard for driving pumps, compressors, and traction. The simple construction of an induction motor lends itself to such applications. This project aims to elaborate on the performance characteristics of a symmetric three-phase induction motor. The analysis carried out is based on the measurable quantities of the machine while referring the rotor variables to the stator.

Induction machines also referred to as asynchronous machines, work on an AC supply. From this perspective, they are like synchronous machines, but the significant difference between the two is that induction machines operate at a speed lower than synchronous speed, while synchronous machines rotate at synchronous speed. This phenomenon is called slip and forms the backbone of the inductive effect. Due to the simple structure of induction machines, they are inexpensive. Thus, they have been utilized widely in various applications. Their tolerance for low maintenance and repair proves advantageous in areas with harsh environments.

In this paper, the induction machine will be studied under free acceleration conditions with minimal damping. Consequently, when the speed reaches a steady state, the torque drops to zero. The structure of induction motors differs entirely from its DC counterpart. In the present paper, the model of an induction machine in a static reference frame gives the ability to determine plenty of possible machine variables. A computationally straightforward modeling approach for machine representation is the model obtained from the reference frame theory. It is currently beyond the scope of the study at hand but allows for fewer control variables thereby being more efficient.

A rotating magnetic field is crucial for the three-phase induction machine's operation. The principle involves applying a set of balanced voltages at the windings of the stator that is

shifted by 120°. Additionally, the distribution of the winding conductors is in a sinusoidal manner. Consequently, the currents in the stator windings produce a magnetomotive force due to the excitation. The magnetomotive force is directly proportional to the source input, so they will vary instantaneously. The stator magnetic field is "spinning" at a synchronous speed. Therefore, the resultant magnetic field will be a rotating vector that rotates at the synchronous speed. Unlike DC machines, where voltage and current play a part in determining the speed of rotation, in induction machines, the speed is only governed by the synchronous speed.

The model of an induction motor is developed based on Newton's and Faraday's laws. The equations attained from the analysis are used to create a model of the motor. The implementation consists of a combined MATLAB/Simulink project allowing for a parameterized model. The results are presented and discussed in the successive sections.

The machine in perspective is a wound rotor induction machine, but the same analysis holds true for squirrel cage induction motors. Fig. 1. shows how the frame of reference of this induction machine is employed.

Faraday's law of electromagnetism and Newton's law of mechanical equilibrium form the basis of the mathematical treatment. The objective of this treatment is to obtain a set of equations for simulation. The results from this simulation will represent the characteristics of the machine. Electrical machines are subject to variations; thus, incorporating these data into this model will help in reinforcing the outcome and motivate further enhancement.

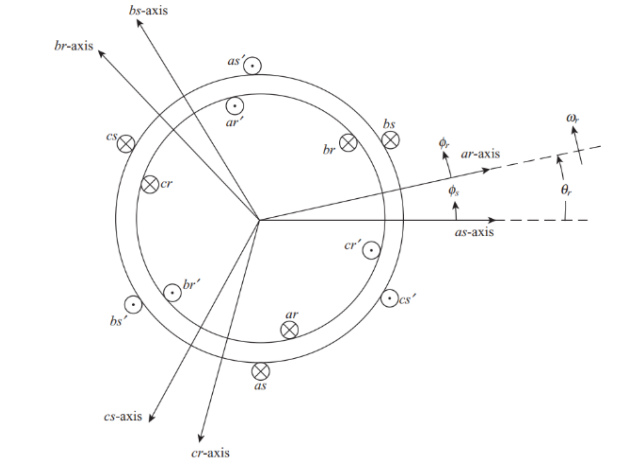

(a) Cross-sectional view of the machine showing the conductors and the axes of reference.

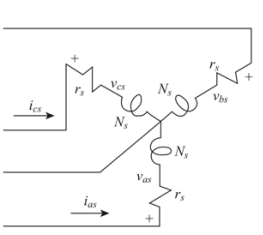

(b) Circuit diagram showing stator windings.

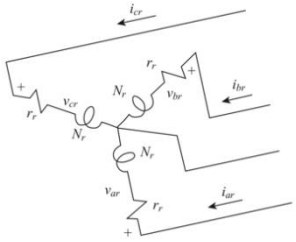

(c) Circuit diagram showing the rotor windings.

Fig. 1. Frame of reference and electrical circuit of motor as taken from [1]

III. Methodology

In this section, a model of the induction machine is defined using state space equations. The derived equations are instrumental in simulating the induction machine and understanding its behavior.

A. Circuit analysis based on Newton's law

According to Kirchhoff's voltage law, the sum of all voltage drops across the circuit is equal to the supply voltage. The back EMF developed due to excitation is given as the rate of change of flux linkage.

$$v(t) = ri(t) + l\frac{di(t)}{dt} + \underbrace{p\lambda}_{e_f} \tag{1}$$

This excitation causes a current to flow through the circuit. It is assumed that the inductance of the wire is zero; therefore, the second term in (1) has a zero value. Since the system of interest is a three-phase induction machine, the flux linkage for each phase needs to be computed. The relation between flux linkages and currents for the phases a/b/c are expressed as a matrix in (2).

$$\begin{bmatrix} \vec{\boldsymbol{\lambda}}_{abcs} \\ \vec{\boldsymbol{\lambda}}'_{abcr} \end{bmatrix} = \begin{bmatrix} \bar{\boldsymbol{L}}_s & \bar{\boldsymbol{L}}'_{sr} \\ (\bar{\boldsymbol{L}}'_{sr})^T & \bar{\boldsymbol{L}}'_r \end{bmatrix} \begin{bmatrix} \vec{\boldsymbol{i}}_{abcs} \\ \vec{\boldsymbol{i}}'_{abcr} \end{bmatrix} \tag{2}$$

Each term in the inductance matrix in (2) is another matrix that depends upon the inductances L_{ls} and L'_{lr} of the stator and the rotor respectively, and the stator magnetizing inductance L_{ms}. Note that the leakage inductance for the rotor is referred to the stator. Equations (3), (4) and (5) define the matrices $\bar{\boldsymbol{L}}_s$, $\bar{\boldsymbol{L}}'_r$ and $\bar{\boldsymbol{L}}'_{sr}$

$$\bar{\boldsymbol{L}}_s = \begin{bmatrix} L_{ls}+L_{ms} & \frac{-L_{ms}}{2} & \frac{-L_{ms}}{2} \\ \frac{-L_{ms}}{2} & L_{ls}+L_{ms} & \frac{-L_{ms}}{2} \\ \frac{-L_{ms}}{2} & \frac{-L_{ms}}{2} & L_{ls}+L_{ms} \end{bmatrix} \tag{3}$$

$$\bar{\boldsymbol{L}}'_r = \begin{bmatrix} L'_{lr}+L_{ms} & \frac{-L_{ms}}{2} & \frac{-L_{ms}}{2} \\ \frac{-L_{ms}}{2} & L'_{lr}+L_{ms} & \frac{-L_{ms}}{2} \\ \frac{-L_{ms}}{2} & \frac{-L_{ms}}{2} & L'_{lr}+L_{ms} \end{bmatrix} \tag{4}$$

$$\bar{\boldsymbol{L}}'_{sr} = L_{ms} \begin{bmatrix} \cos\theta_r & \cos\left(\theta_r+\frac{2\pi}{3}\right) & \cos\left(\theta_r-\frac{2\pi}{3}\right) \\ \cos\left(\theta_r-\frac{2\pi}{3}\right) & \cos\theta_r & \cos\left(\theta_r+\frac{2\pi}{3}\right) \\ \cos\left(\theta_r+\frac{2\pi}{3}\right) & \cos\left(\theta_r-\frac{2\pi}{3}\right) & \cos\theta_r \end{bmatrix} \tag{5}$$

The rotor's leakage inductance L'_{lr} as referred to the stator is expressed by (6) in terms of the number of stator and rotor windings N_s and N_r respectively.

$$L'_{lr} = \left(\frac{N_s}{N_r}\right)^2 L_{lr} \tag{6}$$

Furthermore, inductance can be calculated from reactance using (7)

$$L = \frac{X}{\omega_E} \tag{7}$$

The expression for flux linkages from (2) is substituted in (1) to obtain a relation between supply voltage and winding currents as given below.

$$\begin{bmatrix} \vec{V}_{abcs} \\ \vec{V'}_{abcr} \end{bmatrix} = \begin{bmatrix} \bar{r}_s + p\bar{L}_s & p\bar{L'}_{sr} \\ p(\bar{L'}_{sr})^T & \bar{r'}_r + p\bar{L'}_r \end{bmatrix} \begin{bmatrix} \vec{i}_{abcs} \\ \vec{i'}_{abcr} \end{bmatrix} \tag{8}$$

The rotor's resistance $\bar{r'}_r$ as referred to the stator is calculated by (9).

$$\bar{r'}_r = \left(\frac{N_s}{N_r}\right)^2 \bar{r}_r \tag{9}$$

B. Circuit analysis based on Newton's law

The electromagnetic torque generated by the induction machine depends on the currents in the stator and the rotor and is defined in (10). The derivation of this equation and can be referred from [1].

$$T_e = \left(\frac{P}{2}\right) (\vec{i}_{abcs})^T \frac{\partial}{\partial \theta_r} [\bar{L'}_{sr}] \vec{i'}_{abcr} \tag{10}$$

The value of $\bar{L'}_{sr}$ can be substituted from (5) into (10) to obtain an expression for T_e as shown in (11). The expression is large and is hence divided into sections.

$$\begin{aligned} T_e &= \left(\frac{-PL_{ms}}{2}\right)\{(G_a + G_b)\sin\theta_r + G_r \cos\theta_r\} \\ G_a &= i_{as}\left(i'_{ar} - \frac{(i'_{br} + i'_{cr})}{2}\right) + i_{bs}\left(i'_{br} - \frac{(i'_{ar} + i'_{cr})}{2}\right) \\ G_b &= i_{cs}\left(i'_{cr} - \frac{(i'_{br} + i'_{ar})}{2}\right) \\ G_r &= \frac{\sqrt{3}\,[i_{as}(i'_{br} - i'_{cr}) + i_{bs}(i'_{cr} - i'_{ar}) + i_{cs}(i'_{ar} - i'_{br})]}{2} \end{aligned} \tag{11}$$

The electromagnetic torque T_e and the rotor speed ω_r are related by (12)

$$T_e = J\left(\frac{2}{P}\right) p\omega_r + T_L \tag{12}$$

The synchronous speed is a function of the supply frequency and the pole count and is given in (13) along with the calculations for this model.

$$N_s = \frac{120 \times f}{P}$$

$$N_s = \frac{120 \times 60}{4} = 1800 \text{ rev/min} \tag{13}$$

C. Power analysis

The power dissipated by the windings can be calculated through resistive losses and are added together to represent the loss of all phases. Equation (14) represents the generalized formula for resistive losses.

$$P_d(W) = i^2 r \tag{14}$$

The power generated in horsepower at the shaft of the machine can be calculated using (15).

$$P(W) = \omega_r \times T_e \tag{15}$$

The instantaneous power flowing into the machine is a product of the voltage applied at the terminals and the current flowing into the stator windings for each phase.

$$P_{inp}(W) = V_{ph} \times i_{ph} \tag{16}$$

IV. Modeling

This section attempts to simulate a three-phase four-pole induction machine under free acceleration. Therefore, a three-phase AC voltage is provided to the stator throughout the simulation. Since the machine is being observed under free acceleration, the load torque is set to zero with minimal rotor damping. The machine is assumed to be initially at rest. Consequently, the stator and rotor currents $\vec{i}_{abcs}$ and $\vec{i'}_{abcr}$ and the torque T_e are determined during the simulation. The various machine parameters required for the simulation are quantified in Table II. For implementing the Faraday's law, the provided winding reactances are converted to inductances using (7).

For simulating the induction machine, relationships are derived using both Faraday's Law (8) and Newton's Law (11) in conjunction to observe system operation. In constructing the simulation for Faraday's Law, Fig. 2 is utilized. The model subsystem simulates the winding current for a single phase. Therefore, the subsystem design needs to be appropriately

TABLE II
INDUCTION MACHINE PARAMETERS

Parameter	Value
v	$460V_{rms}$
P	4
ω_B	377 rad/s
ω_E	377 rad/s
r_s	0.087 Ω
r'_r	0.228 Ω
X'_{lr}	0.302 Ω
X_{ls}	0.302 Ω
X_M	13.8 Ω
J	$1.662 kg.m^2$
B	0.00001

replicated for each phase of the rotor and the stator. In constructing the simulation for Newton's Law, Fig. 3 is utilized. The winding currents obtained from Faraday's Law are utilized to calculate the electromagnetic torque T_e.

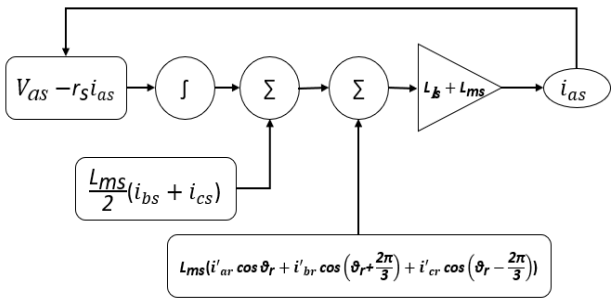

Fig. 2. Faraday's Law for 3-phase induction machine

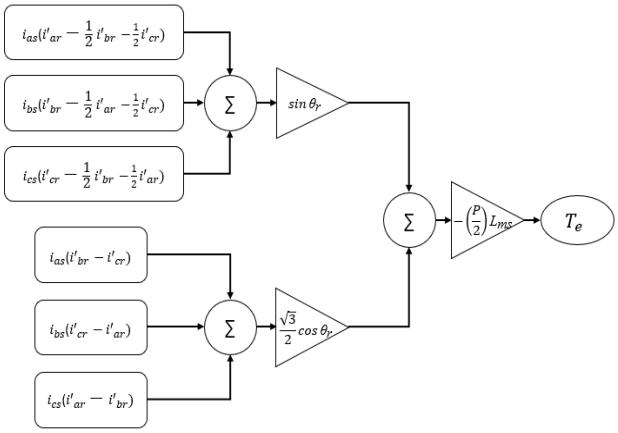

Fig. 3. Newton's Law for 3-phase induction machine

The system states of the induction machine change rapidly in the transient state and change slowly as the system approaches a steady state. Hence, a variable step solver is used with the Dormand-Prince configuration (Ode45) to adapt the step size according to the rate of change in states. The values of the simulation parameters used are specified in Table III.

TABLE III
INITIAL MACHINE PARAMETERS

Simulation parameter	Value
Step size	Variable step size
Solver	ode45 (Dormand Prince)
Stop time (s)	~ 0.3
Maximum step time (s)	Auto
Minimum step time (s)	1 x 10^{-4}

V. RESULTS

This section focuses on the performance plots obtained through simulation. As discussed earlier, "abc" variables represent the phases on the stator and rotor. It is necessary to achieve matching plots to verify the model's accuracy as in [1]. For this condition, the induction machine is being simulated with a zero-load torque on the machine's shaft. Consequently, the sole input will be the three-phase supply voltage. The following figures depict the trends for a single-phase assuming a balanced system. Fig. 4. and Fig. 5. focus on the performance of the induction machine model, the representation of single-phase current in the rotor and stator. In addition, it also covers the relation of the electromagnetic torque versus the rotor speed.

An advanced analysis involves simulating the model to obtain the transient data. This analysis includes the peak values of stator current, peak torque, and the study of power flow in the machine. The stator and rotor losses dominate the amount of power lost in the conversion.

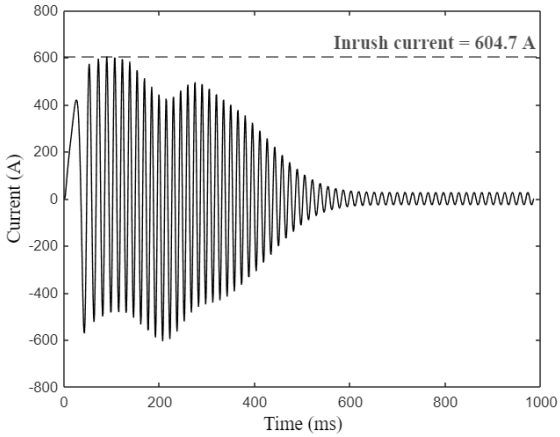

Fig. 4. Single phase stator current showing the large inrush current value

In Fig. 4. the stator's current draw is plotted against time. The induction machine draws the peak stator current of 604.7 A at 53 ms. In addition, the current amplitude decreases as the velocity increases in the motor and finally settles as synchronous speed is reached. It is worth mentioning that when the machine has reached synchronous speed at a steady state, the maximum stator current is 21.8 times higher than the nominal current at no-load conditions. Since the fraction is neglected at the steady-state condition, there is no power transmitted to the shaft due to the free acceleration condition. Therefore, there is no field energy at this state.

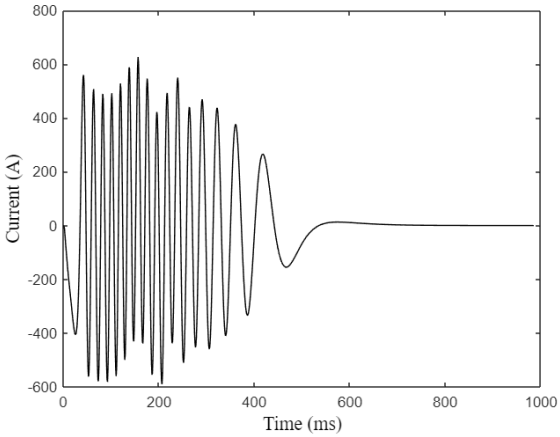

Fig. 5. Rotor current for a single phase

In Fig. 5. the rotor's current performance is illustrated. The peak current attained by the rotor is 626.36A. The value of the rotor current might appear unreasonable, but it is worth bearing in mind that the referred values are a product of the turns ratio, making them appear amplified. The amplitude of the curve before the steady state decreases more drastically than the stator current. The rotor current drops to zero at equilibrium due to the lack of inductive effect. Therefore, the machine is mechanically and electrically spinning at 377 rad/s in the absence of load torque.

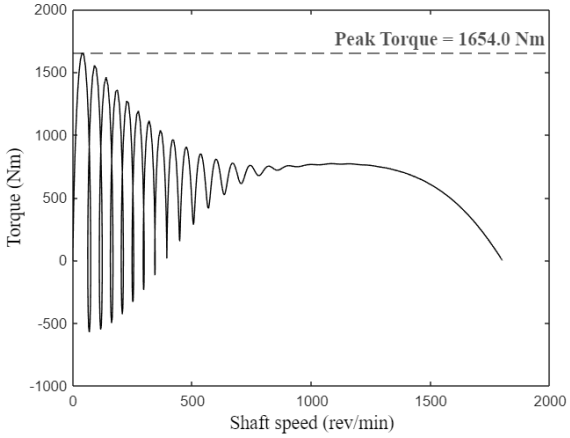

Fig. 6. Torque-speed characteristics showing the peak start-up torque.

The torque-speed characteristics show the progression of the torque as the machine accelerates. The torque reaches its maximum torque going from zero to 1654 Nm upon starting. The curve decays with a rippling behavior until the system settles at the synchronous speed of 1800 rpm. The previous statement affirms that the simulation is accurate. It is essential to cite the importance of illustrating the instantaneous torque instead of the average torque. The main reason for including this plot is that the plateau of this curve is approximately 500 Nm which does not represent the actual nature of the machine's torque. This value is a practical manufacturing benchmark when selecting the integrity of associated materials further down the driveline.

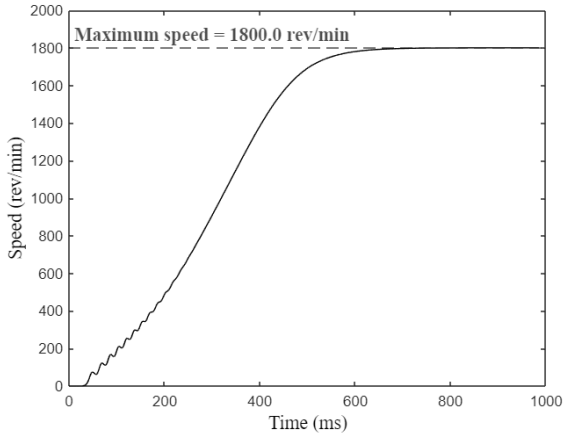

Fig. 7. Speed characteristics

Fig. 7. demonstrates the absolute speed of a four-pole machine. In its initial stages, the motor accelerates while rippling up to 600 rev/min. The steady state is reached when the machine achieves its 1800 rev/min synchronous speed. There is no power transferred to the shaft during the steady-state simulation due to the free acceleration condition. However, it is evident from the stator current draw that the machine still has rotational motion. Keeping a practical scenario in mind, the motor in question can have a minor damping factor.

The subsequent plots probe deeper into the study by illustrating the power characteristics. The variables in the discussion are the instantaneous winding copper losses and output shaft power. These aspects will go a long way in highlighting the efficiency limits imposed due to the machine parameters and thermal impacts caused by the dissipated power.

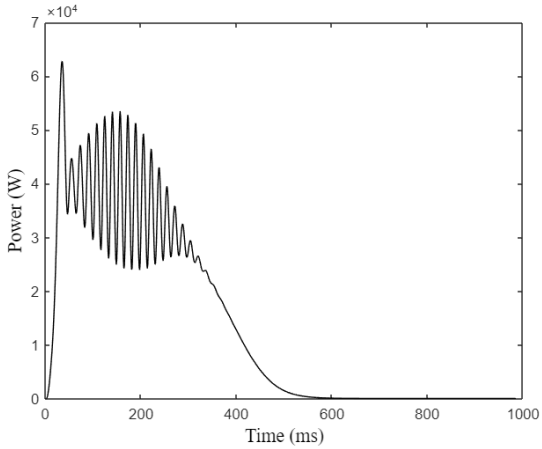

Fig. 8. Dissipated power from stator

The stator resistive losses crest at 62.7 kW for the large inrush current, while the peak ripple amplitude in the transient region is approximately 35 kW. As soon as the torque plateaus, the stator power losses decay practically linearly and further decrease along with the torque.

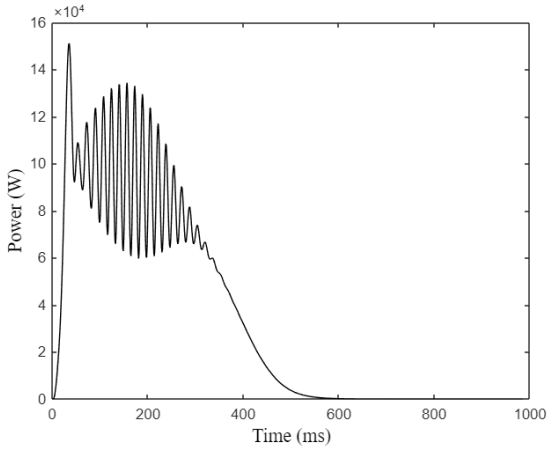

Fig. 9. Dissipated power from rotor

In this case, the dissipated power at the rotor reaches its highest value of 151 kW at 6 ms. Unlike the stator, the dissipated power drops to zero during steady state as the rotor

current drops to zero. While the characteristics in power dissipation for both sets of windings follow similar trends, the power dissipated in the rotor is more than twice the stator dissipation.

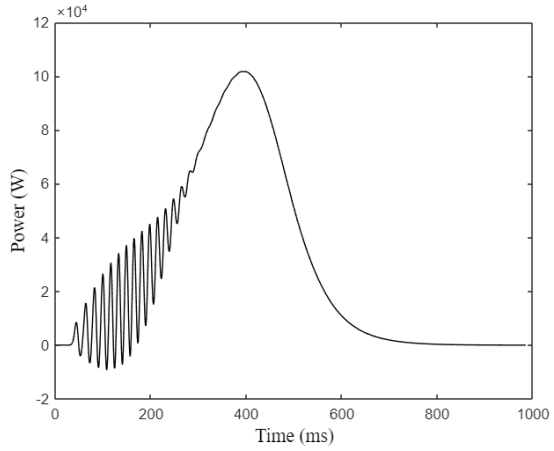

Fig. 10. Shaft power

Fig. 10. illustrates the shaft power. The shaft power is directly correlated with electromagnetic torque and shows a ripple characteristic. While the machine accelerates, the power ripples and rises until it reaches the peak value, then it decreases as the torque decreases while the speed stays constant. The highest power obtained from the machine is 100 kW is at 3.8 ms. Since the damping is minimal, the power drops to negligible amount upon reaching equilibrium

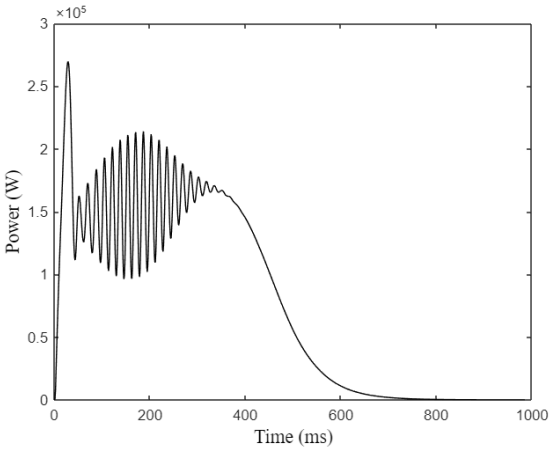

Fig. 11. Total instantaneous power flowing into the machine

The total input instantaneous power is a sum of power drawn by each of the three stator phases multiplied by their respective phase voltages. This power, too, tends to oscillate with the stator winding current. The peak power drawn by the machine is close to 275 kW. Fig. 10. shows the total power drawn.

VI. Analysis and Discussion

The stator current shows a typical trend in induction motors with a severe inrush current. This high starting current is indicative of the resistive nature of the winding that is dominant at lower speeds. As the machine picks up speed, the rate of change of flux linkage increases, thereby setting up a back EMF. This EMF counteracts the supply voltage leading to a decay in the current. This reduction leads to deceleration and reduces the back EMF, increasing the current. This cycle repeats, driving the machine into a self-adjusting process to compensate for the slip.

The rotor currents show similar behavior but reduce to a zero value at the synchronous speed. This behavior comes across as unusual but is a consequence of the diminishing inductive effect at synchronous speed. While this analysis illustrates only one of the phase currents for each set of windings, it is under the assumption that the other phases have similar characteristics, albeit with a phase difference of 120°.

The electromagnetic torque is an outcome of the stator and rotor current. The high starting values of these components give rise to the excessive starting torque, which can exceed the maximum torsional strength of the shaft leading to shearing action. Hence it is appropriate to size the driveline bearings and couplings with peak figures. Also, the ripple introduced in the acceleration phase might lead to vibration of motor mounts, causing shaft misalignments and bearing failures. This problem is compounded if the vibrations are at the resonant frequency of the output shaft, amplifying the vibrations.

The peak value of the stator current is also called the "locked rotor current" This phenomenon is experienced in induction motors in the first few moments upon startup. The peak values of the stator currents play an essential part in deciding the capacity of the inverters used to drive the motor. In the absence of this consideration, the inverters will often trip with over-current warnings. If connected directly to the mains supply, this magnitude of startup current is sure to trip circuit breakers with insufficient capacity. As for the stator currents, a quantifiable value of current can help decide the size of the wire gauge. The gauge has a tremendous impact on two significant characteristics. The primary characteristic is the current-carrying capability. The secondary is the weight and, ultimately the rotor inertia

The resistive losses caused by the inrush currents are incredibly high and place thermal stress on the winding insulation causing premature degradation with the possibility of shorting adjacent windings. Since the loss is an exponential function of the current, a slight rise in the current can lead to significant losses. Similar is the case for the rotor windings. The shaft power shows a rise while going through a similar oscillatory nature. The rise in power can be explained by looking at the speed and torque curves. The torque curve experiences a plateau while the speed rises linearly, leading to an overall spike in the shaft power.

VII. Conclusion

The proposed model of induction machines allows for a holistic modeling scheme that encompasses several aspects ranging from illustrating the winding currents to power analysis. This in-depth analysis is possible due to a parameterized model that combines the simplicity of a graphical approach and the iterative nature of the coding environment. The outcome of this exercise is a mathematically

accurate model capable of depicting the behavior of an induction machine when subject to changing machine parameters. It forms the foundation of further analysis and gives a glimpse at the complexity of control involved in applying the arbitrary frame theory.

VIII. ACKNOWLEDGMENT

The authors thank Dr. Christopher Shannon Edrington for equipping them with the required technical knowledge on induction machines. His valuable and constructive suggestions have helped resolve discrepancies during the initial stages. Also, his constant encouragement has made this project possible despite tight deadlines.

IX. REFERENCES

[1] Paul Krause, Oleg Wasynczuk, Scott Sudhoff, Steven Pekarek, "Analysis of Electric machinery and Drive Systems" 3rd Edition, IEEE press, 445 Hoes Lane, Piscataway, NJ 08854, 2013.

[2] Dr. Christopher S. Edrington, “Class Notes”, ECE 4190-6190 Electrical Machines and Drive Systems.

X. BIOGRAPHIES

Leticia Breton Garcia is a senior electrical engineering major graduating from Universidad Pontificia de Comillas ICAI in Madrid, Spain. She has been studying at Clemson University this past year, which broadened her professional and cultural background.

Shubham Gupta is a graduate student at Clemson University’s International Center for Automotive Research (CU-ICAR). He is passionate about electric powertrains and is currently working on the Deep Orange 14 project to develop the next-gen off-road autonomous vehicle for the US Army.

Sahand Liasi received the B.Sc. and M.Sc. degrees in electrical engineering from K.N. Toosi University of Technology, Tehran, Iran, in 2016 and 2019, respectively. Currently, he is a PhD student at Clemson University. His research interests include smart grids, demand response, power quality, and power electronics.

Saumil Pradhan is a graduate student at Clemson University’s International Center for Automotive Research Campus at Greenville, SC. He is specializing in the Advanced Powertrains and Drivelines track and wants to pursue a career as a Controls Engineer. He is also part of the Deep Orange 14 team, one of the flagship programs of the automotive engineering department.

Pranav Ghate is currently pursuing a Graduate degree in Electrical Engineering at Clemson university. He has received his bachelor’s degree in Electronics and Telecommunication Engineering from Savitribai Phule Pune Institute, Pune, India. His experience includes working on armored vehicles utilized by the Indian Army and with fleet management systems for public transport vehicles. His interest includes a gamut of concepts from drives and advanced power electronics to transport electrification.